

Towards Thermally Regenerative All-Copper Redox Flow Battery

Pekka Peljo,^{1,2} David Lloyd,^{1,*} Nguyet Doan,¹ Marko Majaneva,¹ and Kyösti Kontturi¹

¹Aalto University, Department of Chemistry B.O. Box 16100, 00076 Aalto, Finland

²Laboratoire d'Electrochimie Physique et Analytique, Ecole Polytechnique Fédérale de Lausanne (EPFL), Station 6, 1015 Lausanne, Switzerland.

*Corresponding author

Tel. +358 50 3435462

Fax +358 9 47022580

Email david.lloyd@aalto.fi

1 Design of the miniature redox flow battery

To be able to do initial measurements with redox flow batteries, the use of permeability cells was found to be ideal. The structure of a permcell based redox flow battery is shown in figure S-1. The system is similar to the H-cells conventionally used for preliminary flow battery studies. The electrolyte is not flowing in the system; the electrodes are in direct contact with the electrolyte reservoirs instead. This design minimizes the ingress of oxygen in to the cell, as it would oxidize the reduced species. The design also facilitates precise temperature control and reduces both the size of the electrodes and the amount of electrolyte required. Importantly, since the material of construction of the two half-cells is glass, continual observation of the state of the electrode surface is possible. Integration of the electrolyte storage and convection in to the same space as the electrodes results in an extremely simple design. PermeGear Side-Bi-Side glass diffusion cells (interfacial area of 0.636 cm^2) mounted on a H3 3-Station cell stirrer (500 rpm), with FAB or Nafion membrane clamped between the cells was used. The temperature of the cell was controlled by connecting the jackets of the cells into the external thermal bath.

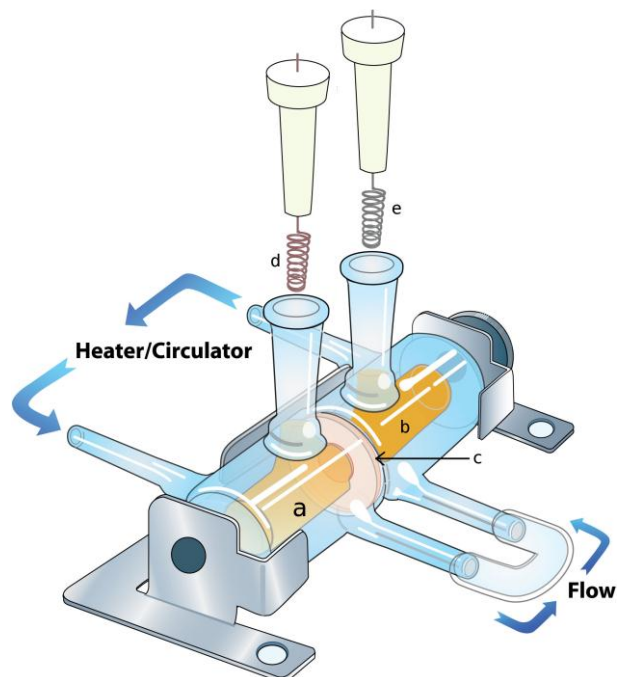


Figure S1. Illustration of the redox battery system utilised in this communication. a and b are the two jacketed half-cells,, where the electrolyte is shown in yellow, c is the ion exchange membrane which prevents mixing of the electrolytes in the two half-cells. d and e are the two electrodes, which pass through a polypropylene stopper to ensure tight sealing. Convection is maintained by a pair of magnetic stirrers rotating in close proximity to the electrodes at 500 rpm. The heating fluid from the thermal bath flows through the jacket of the compartment a and then through the jacket of the compartment b.

2 Cycling Performance of the All-Copper Redox Flow Battery

Figure S2 shows the typical iR -corrected charge-discharge cycles obtained with the miniature redox flow battery for Pt cathode and FAB membrane, 5 cycles at the current density of 7.86 mA cm^{-2} followed by 5 cycles at the current density of 15.7 mA cm^{-2} , 5 cycles at 7.86 mA cm^{-2} . Figure S3 shows the following cycles at the current density of 1.57 mA cm^{-2} .

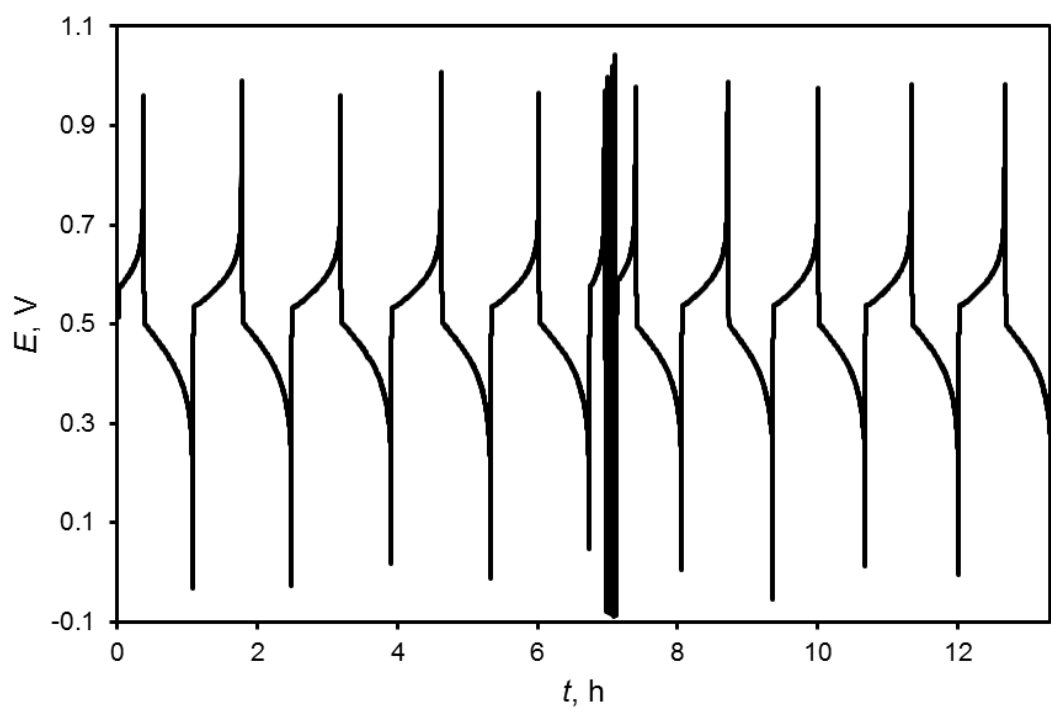


Figure S2. Cycling behavior of the miniature redox flow battery (0.1 M CuSO_4 + 0.5 M H_2SO_4 in 6 M acetonitrile) with Pt cathode and FAB membrane, first cycles at 7.86 mA cm^{-2} followed by 5 cycles at 15.7 mA cm^{-2} and 5 cycles at 7.86 mA cm^{-2} .

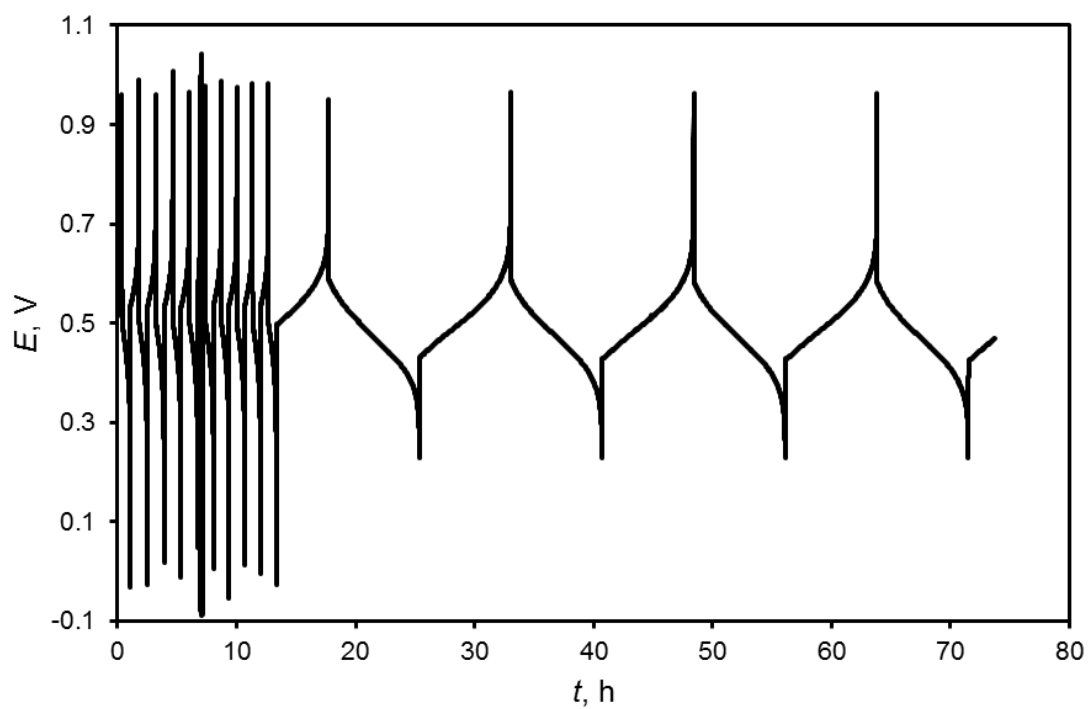


Figure S3. Cycling behavior of the miniature redox flow battery (0.1 M CuSO_4 + 0.5 M H_2SO_4 in 6 M acetonitrile) with Pt cathode and FAB membrane, discharge cycling shown in Fig. S2 followed by cycling at 1.57 mA cm^{-2} .

It can be seen from Figures S3 and S4 that current density of 15.7 mA cm^{-2} is too high for the battery. At 7.86 mA cm^{-2} the cut-off voltages are more unstable due to the sharp change of the cell potential in the end of charge or discharge. This leads to variation of the coulombic efficiency, as show in Figure 2 of the main text. Figure S4 shows the battery capacity during cycling with different current densities. Discharge curves at the start and after a change in the cycling current are omitted. The results show that the performance of the cell gradually decreases during cycling at 7.86 mA cm^{-2} , but the capacity is more stable at low currents (1.57 mA cm^{-2}).

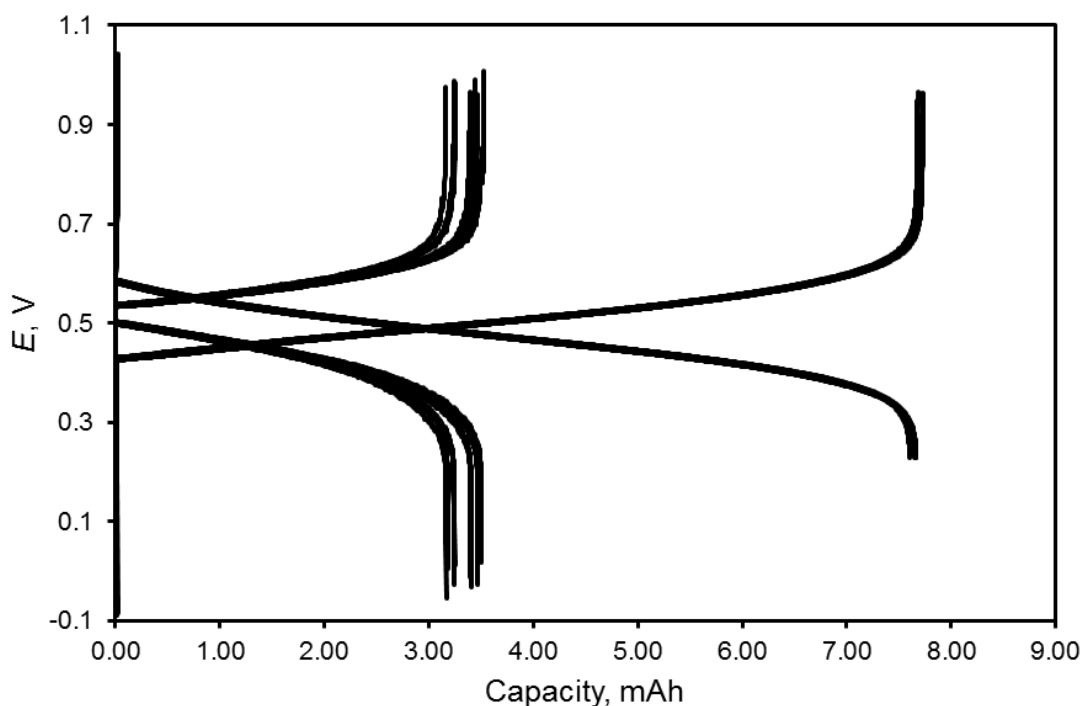


Figure S4. iR corrected voltage as a function of the cell capacity during cycling at different current densities (7.86 mA cm^{-2} and 1.57 mA cm^{-2}).

3 Calculation of the Theoretical Capacity, Coulombic Efficiency and Energy Efficiency

The theoretical capacity of the battery was calculated based on Cu^{2+} content. For complete discharge, all the Cu^{2+} is converted to Cu^+ . From Faraday's law of electrolysis (Equation S-1)

$$Q_{\text{theory}} = nF = cVF \quad (\text{S-1})$$

where Q is charge, n is molar amount of copper(II), F is the Faraday constant, V is volume of the half-cell (3.4 ml) and c is copper(II) concentration (0.1 M). This simple calculation gives the theoretical capacity of the battery (as there is an excess of copper) as 32.8 C or 9.11 mAh.

Charge cycling of the miniature redox flow battery was done by applying a constant current and switching at defined potentials. Integration of the current allows us to quantify the amount of charge passed during the charging and discharging stages, Q_{charge} and $Q_{\text{discharge}}$ respectively. The Coulombic efficiency for each cycle is then as defined in equation S-2.

$$\eta_Q = \frac{Q_{\text{discharge}}}{Q_{\text{charge}}} \quad (\text{S-2})$$

Also we can define the discharge capacity, which is the amount of charge withdrawn from the battery during any given cycle before the applicable switching potential condition is triggered, normalised by the theoretical capacity of the battery, Q_{theory} .

An important, but more problematic parameter to define when examining an RFB based on non-aqueous solvents is the energy efficiency of single charge-discharge cycle, η_E . The Ohmic losses are often significant in non-aqueous systems (in this case 31 Ω) and therefore the use of simple test systems which are not optimized to

minimize these losses, such as the permeability cells used in this communication, could lead to entirely incorrect conclusions regarding the energy efficiency achievable in a real system based on the same electrolytes. For this reason in this communication the energy efficiency is calculated once the cell potential has been corrected for the Ohmic losses using equation S-3 and then summated using S-4:

$$E = E_{\text{obs}} - iR \quad (\text{S-3})$$

where E_{obs} is the observed potential, i is the current and R is the measured resistance.

$$\eta_E = \frac{\sum_{t=t_{\text{switch}}}^{t=t_{\text{end}}} E i_{\text{discharge}} \Delta t}{\sum_{t=0}^{t=t_{\text{switch}}} E i_{\text{charge}} \Delta t} \quad (\text{S-4})$$

where t_{switch} is the time when the voltage constraint for charge is reached and discharging starts, and t_{end} is the time when the voltage constrain for discharge is reached. Δt is the time step.

4 Mutual Solubility of Acetonitrile and CuSO_4 in Aqueous Solutions

Since the mutual solubility of acetonitrile and CuSO_4 appeared to place a low upper limit on the concentration of the electroactive species in the system, experiments were performed to quantify the ternary phase behavior.

This was performed using the cloud point method. Aqueous solutions of $\text{CuSO}_4 \cdot 5\text{H}_2\text{O}$ were prepared at differing concentrations (total mass $\sim 20\text{g}$). These were placed in an air-tight glass vessel (thermostated at $25\text{ }^\circ\text{C}$) and acetonitrile was slowly added using a Schott titronic basic digital titrator until the cloud point was observed. The accuracy of this method was validated by performing a series of measurements using NaSO_4 and comparing these with literature values.¹

For solutions with a low concentration of copper sulfate content the formation of a second phase was observed as the formation of a solid copper sulfate precipitate, for solutions rich in copper sulfate a separate acetonitrile rich liquid phase was observed. As is clear from figure S5, copper sulfate is poorly soluble in acetonitrile-water mixtures. This appears to be primarily attributable to the sulfate anion, since lithium sulfate also shows significantly lower solubility than the chloride salt.

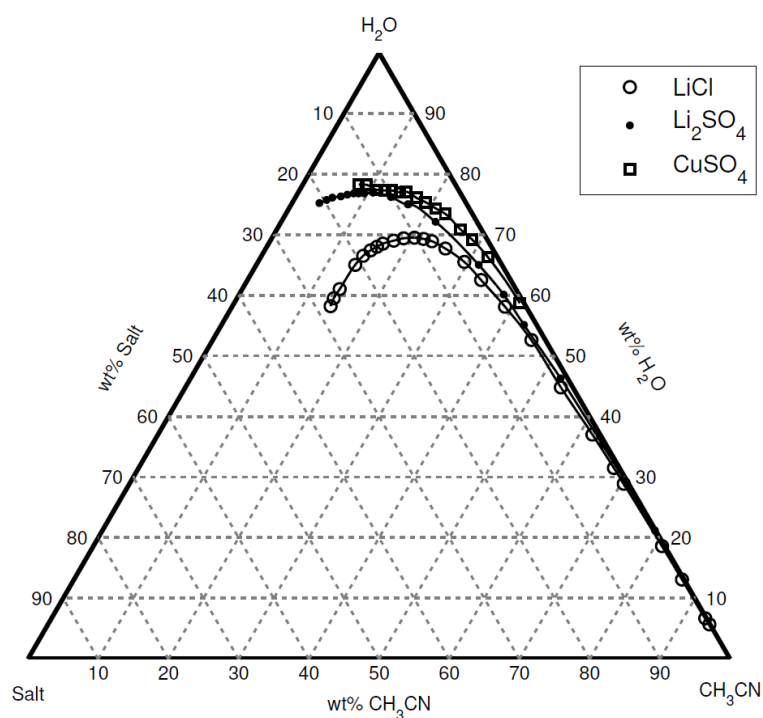


Figure S5. Ternary phase diagram for water-acetonitrile-salts, the data for LiCl and Li₂SO₄ are taken from the literature.² The data for CuSO₄ is presented in table S1.

The selection of a suitable, monovalent, non-complexing anion may allow the use of higher copper concentrations, which would improve current densities.

Table S1. Binodal data for acetonitrile-CuSO₄-water system, as presented in figure S5.

Acetonitrile, wt%	CuSO ₄ , wt%	H ₂ O, wt%
7.96	13.81	78.24
9.05	12.73	78.21
11.07	11.56	77.37
12.19	10.54	77.27
13.19	9.55	77.26
14.46	8.55	76.99
15.31	7.62	77.07
17.33	6.61	76.06
18.99	5.67	75.33
20.92	4.74	74.33
22.69	3.87	73.45
26.2	2.95	70.85
28.68	2.14	69.18
32.35	1.35	66.3
40.7	0.59	58.7

5 References

1. J. Renard, *J. Chem. Eng. Data*, 1966, **11**, 169-171.
2. J. Renard, *J. Chem. Eng. Data*, 1967, **12**, 33-36.